Author's personal copy

Remote Sensing of Environment 113 (2009) 730–744

Contents lists available at ScienceDirect

Remote Sensing of Environment

journal homepage: www.elsevier.com/locate/rse

Modelling PRI for water stress detection using radiative transfer models

L. Suárez [a], P.J. Zarco-Tejada [a,*], J.A.J. Berni [a], V. González-Dugo [a], E. Fereres [a,b]

[a] Instituto de Agricultura Sostenible (IAS), Consejo Superior de Investigaciones Científicas (CSIC), Córdoba, Spain
[b] Department of Agronomy, University of Cordoba, Campus Universitario de Rabanales, 14014 Córdoba, Spain

ARTICLE INFO

Article history:
Received 26 May 2008
Received in revised form 5 December 2008
Accepted 5 December 2008

Keywords:
Water stress
Photochemical Reflectance Index
PRI
Multispectral remote sensing
Thermal
Radiative transfer modelling

ABSTRACT

This paper presents a methodology for water stress detection in crop canopies using a radiative transfer modelling approach and the *Photochemical Reflectance Index* (PRI). Airborne imagery was acquired with a 6-band multispectral camera yielding 15 cm spatial resolution and 10 nm FWHM over 3 crops comprising two tree-structured orchards and a corn field. The methodology is based on the PRI as a water stress indicator, and a radiative transfer modelling approach to simulate PRI baselines for non-stress conditions as a function of leaf structure, chlorophyll concentration (Cab), and canopy leaf area index (LAI). The simulation work demonstrates that canopy PRI is affected by structural parameters such as LAI, Cab, leaf structure, background effects, viewing angle and sun position. The modelling work accounts for such leaf biochemical and canopy structural inputs to simulate the PRI-based water stress thresholds for non-stress conditions. Water stress levels are quantified by comparing the image-derived PRI and the simulated non-stress PRI (sPRI) obtained through radiative transfer. PRI simulation was conducted using the coupled PROSPECT-SAILH models for the corn field, and the PROSPECT leaf model coupled with FLIGHT 3D radiative transfer model for the olive and peach orchards. Results obtained confirm that PRI is a pre-visual indicator of water stress, yielding good relationships for the three crops studied with canopy temperature, an indicator of stomatal conductance (r^2=0.65 for olive, r^2=0.8 for peach, and r^2=0.72 for maize). PRI values of deficit irrigation treatments in olive and peach were consistently higher than the modelled PRI for the study sites, yielding relationships with water potential (r^2=0.84) that enabled the identification of stressed crowns accounting for within-field LAI and Cab variability. The methodology presented here for water stress detection is based on the visible part of the spectrum, and therefore it has important implications for remote sensing applications in agriculture. This method may be a better alternative to using the thermal region, which has limitations to acquire operationally high spatial resolution thermal imagery.

© 2008 Elsevier Inc. All rights reserved.

1. Introduction

The *Photochemical Reflectance Index* (PRI) was proposed by Gamon et al. (1992) as an indicator of the de-epoxidation state of the xanthophyll pigments related with photosynthetic processes. It is based on a normalized difference of the 530 nm band where xanthophyll pigment absorption occurs, and a reference band located at 570 nm. As the xanthophyll pigments are related to light absorption mechanisms, the PRI index has been extensively linked to light use efficiency (LUE) at the leaf scale (Guo & Trotter, 2004; Nakaji et al., 2006; Serrano & Peñuelas, 2005; Sims et al., 2006), at canopy scale using field spectrometers (Nichol et al., 2000, 2002; Strachan et al., 2002; Trotter et al., 2002) and using satellite imagery such as EO-1 Hyperion (Asner et al., 2005), MODIS (Drolet et al., 2005) and AVIRIS (Fuentes et al., 2006). The estimation of LUE through the remote sensing PRI index has shown a direct link to photosynthesis rate assessment (Guo & Trotter, 2004; Nichol et al., 2000, 2006; Sims et al., 2006). In addition, photosynthesis has also been related to PRI through chlorophyll fluorescence and non-photochemical quenching (Evain et al., 2004; Nichol et al., 2006).

The early detection of water stress is a key issue to avoid yield loss, which can be affected even by short-term water deficits (Hsiao et al., 1976). The pre-visual detection of water stress has been successfully achieved with remote sensing data using thermal infrared radiation since long ago (Cohen et al., 2005; Idso et al., 1978; 1981; Jackson et al., 1977, 1981; Jackson & Pinter, 1981; Leinonen & Jones, 2004; Möller et al., 2007; Sepulcre-Cantó et al., 2006, 2007; Wanjura et al., 2004), and more recently being suggested the visible spectral region with the PRI index as an indicator of stress (Peguero-Pina et al., 2008; Suárez et al., 2008; Thenot et al., 2002). Alternatively, thermal imagery acquired over vegetation is sensitive to canopy transpiration because temperature is raised due to the reduction in evaporative cooling under stress conditions. Thermal remote sensing of water stress has

* Corresponding author. Instituto de Agricultura Sostenible (IAS), Consejo Superior de Investigaciones Científicas (CSIC), Alameda del Obispo, s/n, 14004 — Córdoba, Spain. Tel.: +34 957 499 280, +34 676 954 937; fax: +34 957 499 252.
E-mail address: pzarco@ias.csic.es (P.J. Zarco-Tejada).
URL: http://www.ias.csic.es/pzarco (P.J. Zarco-Tejada).

0034-4257/$ – see front matter © 2008 Elsevier Inc. All rights reserved.
doi:10.1016/j.rse.2008.12.001

Author's personal copy

been accomplished using spectrometers at ground level (Idso et al., 1981; Jackson et al., 1977, 1981), thermal sensors at image level (Cohen et al., 2005; Leinonen & Jones, 2004; Sepulcre-Cantó et al., 2007) and using satellite thermal information (Sepulcre-Cantó et al., in press).

It is well known that severe water deficits affect many physiological processes and have a strong impact on yield (Hsiao et al., 1976). However, even moderate water deficits, which are not easy to detect, can also have important negative effects on yield (Hsiao & Bradford, 1983). It is important to be able to assess the level of stress through some pertinent indicators. This is the case of the xanthophyll cycle response to stress tracked by the PRI index, which is suggested as a pre-visual indicator of water stress and is the aim of this study. PRI has been used to assess pre-visual water stress in the work by Thenot et al. (2002) and Winkel et al. (2002) at leaf level, at canopy level (Dobrowsky et al., 2005; Evain et al., 2004; Peguero-Pina et al., 2008; Sun et al., 2008) and using airborne imaging spectroscopy (Suárez et al., 2008). Both indicators, canopy temperature and PRI, are complementary; they provide physiological information related to plant water status, transpiration and photosynthesis. High spatial resolution imagery in the visible and near infrared region is relatively easy to acquire with current airborne and satellite sensors, such as AHS, Hymap, CASI, AVIRIS, and Hyperion, among others. On the contrary, high-resolution thermal sensors are not common due to technical limitations of microbolometer technology. Moreover, high resolution thermal imagers onboard satellite platforms are restricted due to technical limitations. Current thermal medium resolution sensors on satellite platforms are limited to ASTER and LANDSAT sensors, offering spatial resolutions limited to the 60–120 m pixel-size range. These current technical limitations for acquiring high-spatial resolution thermal imagery emphasize the need for developing pre-visual water stress indicators in the VIS/NIR region for agricultural and precision farming methods. Technically, CMOS and CCD VIS/NIR imaging sensors based on silicon detectors provide very high spatial resolution with pixel sizes at the centimetre level and cost-effective for precision agriculture imagers and future satellite platforms. Thus, attention must be placed on VIS/NIR narrow-band indicators of pre-visual stress, such as PRI, as well as chlorophyll fluorescence for stress-detection methods (Dobrowsky et al., 2005; Pérez-Priego et al., 2005; Suárez et al., 2008; Thenot et al., 2002). Nevertheless, the PRI index cannot be readily used to map vegetation stress without considering leaf and canopy structural effects on the index. PRI bands at 531 and 570 nm are affected by both leaf and canopy parameters such as chlorophyll content (Cab), dry matter (Cm), leaf thickness, leaf area index (LAI), and leaf angle distribution function (LADF), among others (Barton & North, 2001; Suárez et al., 2008). Thus, PRI maps obtained over canopies with variable LAI mask the sensitivity of the index to stress, mostly tracking the spatial variation of the canopy leaf area density and structure (Barton & North, 2001; Suárez et al., 2008). Consequently, modelling work at leaf and canopy scale is needed to enable an operational application of PRI to map water stress in non-homogeneous canopies where structural changes play the main role in the reflectance signature.

A new modelling method is presented in this paper based on radiative transfer simulation to estimate a theoretical PRI baseline

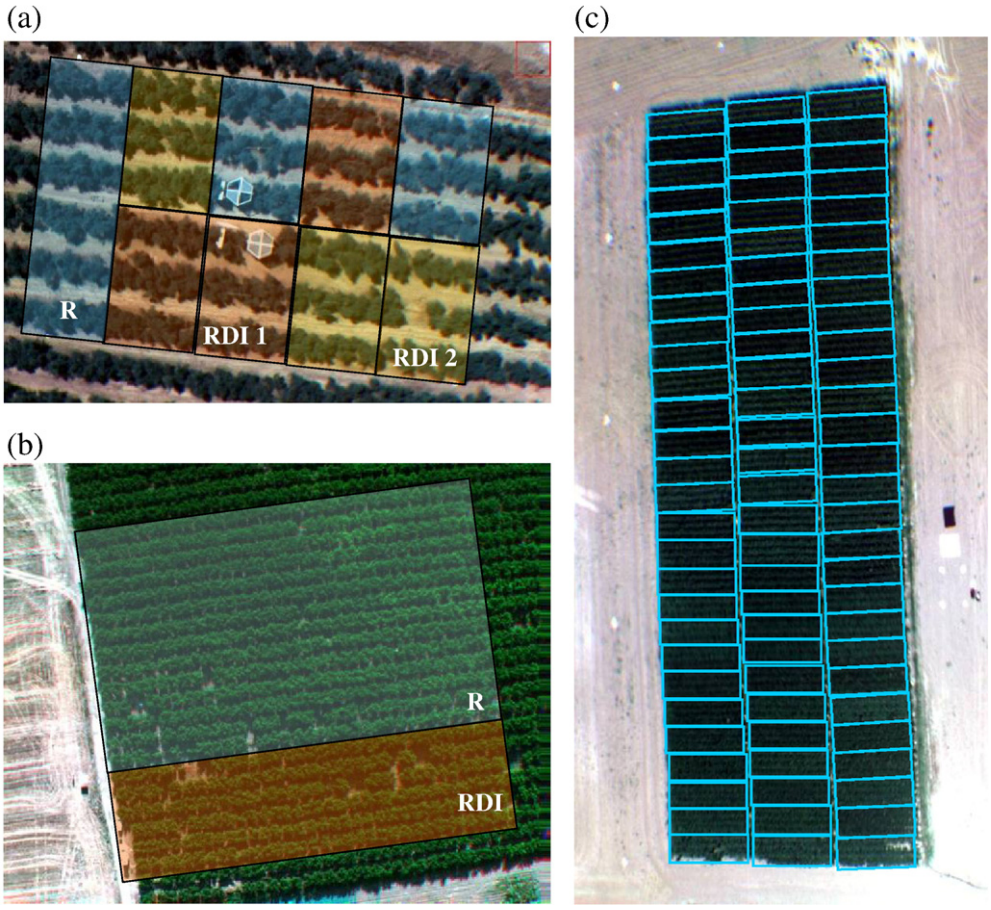

Fig. 1. Overview of the field experiments presented in this study: (a) olive orchard and the three irrigation treatments applied: Full irrigation (R), and two regulated deficit irrigation treatments (RDI1, RDI2); (b) peach orchard with one full irrigation treatment (R) and a regulated deficit irrigation treatment (RDI); and (c) corn field with 24 different cultivars replicated three times.

Author's personal copy

for non-stress conditions for two tree species, olive and peach, and for an herbaceous continuous canopy of maize. The method compares imaged PRI with theoretical non-stress PRI obtained through model inversion for existing structural and background conditions, defining a within field threshold to detect stressed vegetation.

2. Methods

2.1. Study sites

The three main study sites used for field and airborne data collection are located in Córdoba, southern Spain (37.8°N, 4.8°W), on soils classified as Typic Xerofluvents. The climate is Mediterranean with an annual rainfall of 650 mm concentrated between autumn and spring. The first study site corresponds to a 4 ha irrigated-olive orchard (*Olea europaea* L. cv. "Arbequino") established in 1997 in a 3.5×7 m grid. The tree lines follow a north–south direction and the trees were planted on ridges to avoid flooding. The soil had a sandy stratum at 1.5 m and was kept under no-tillage with herbicides. The experiment was designed in an area of six rows where three drip-irrigation treatments were applied, differing in water amounts: (i) constant application rate of 2.8 mm/day during the irrigation season (enough to meet the tree demand, this treatment was used as a reference, R), (ii) application rate of 0.7 mm/day (deficit treatment RDI1), and (iii) an application rate of 1.2 mm/day during the periods between 14 June to 5 July, and from 6 September to 19 October (deficit treatment RDI2). Additional information about the study site and the experiments can be found in previous publications (Pérez-Priego et al., 2005; Sepulcre-Cantó et al., 2006). Fig. 1a depicts the olive orchard and the treatment block location within the olive grove.

The second study site was within a commercial peach orchard (*Prunus persica* cv. "BabyGold8") planted in 1990 in north–south direction in a 5×3.3 m grid on a loam soil without restrictions for root growth down to 3 m depth. A subset of 6 lines×30 peach trees each were irrigated differently than the rest of the orchard. The non-stressed trees were drip irrigated starting on 18th May 2007 with an application rate equivalent to 80% of calculated crop ET. The regulated deficit irrigation treatment (RDI) started irrigation on 5th July at Stage III of fruit development (rapid growth stage) over-irrigating afterwards until tree water status was fully recovered.

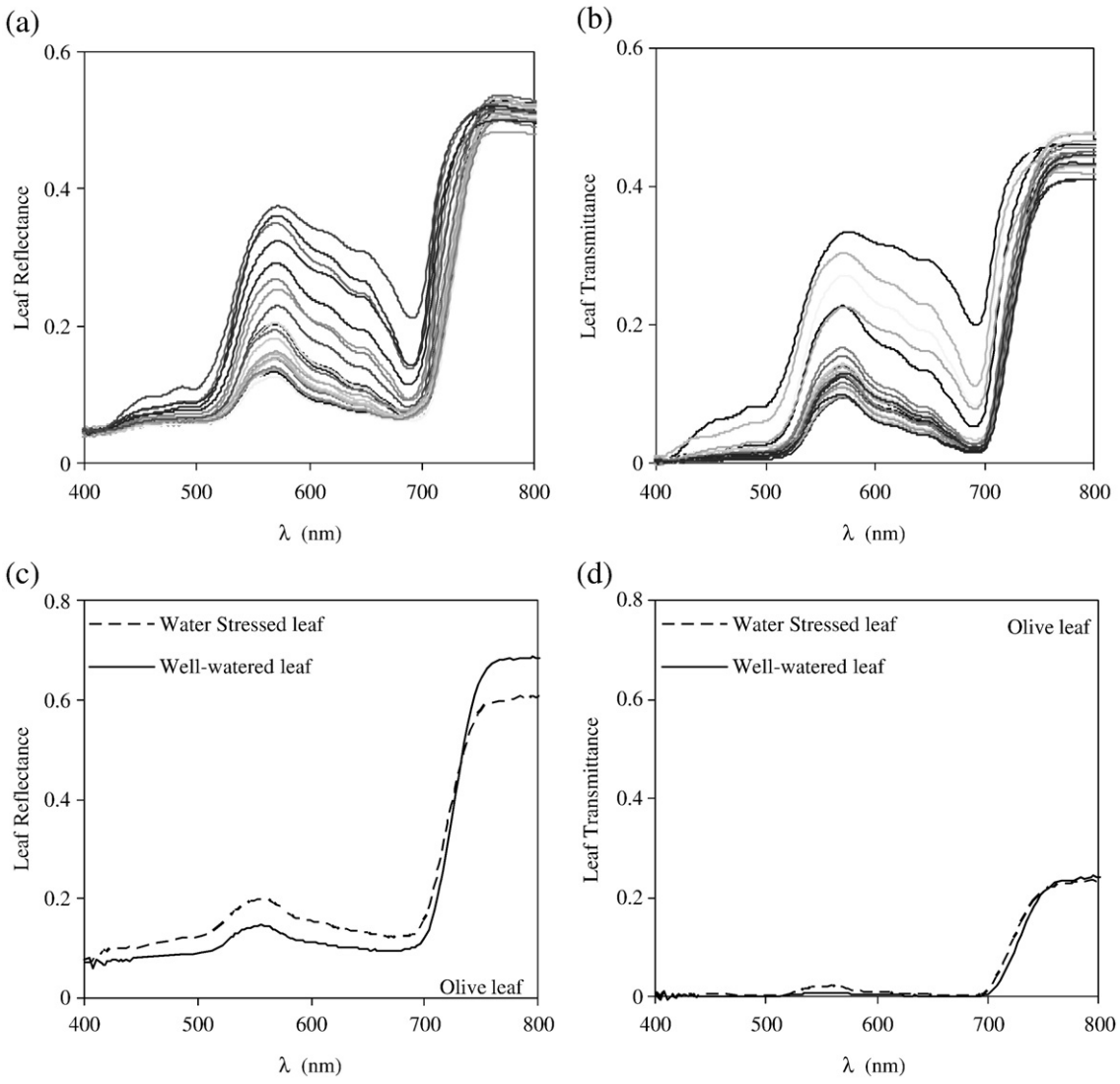

Fig. 2. Leaf reflectance and transmittance measurements taken with an integrated sphere corresponding to a subsample of 30 spectra measured on peach leaves (a and b). Reflectance and transmittance corresponding to water-stressed and well-watered olive leaves (c and d).

Author's personal copy

The concept of regulated deficit irrigation (RDI) was first proposed by Chalmers et al. (1981) to control vegetative growth in peach orchards applying water deficits that did not reduce economic yield (Fereres & Soriano, 2007).

The third study site consisted on a maize field that had 24 varieties replicated three times, yielding a total of 72 plots of 3 m×9 m area. Irrigation had not been applied prior to image acquisition on 6th of June 2007. Afterwards, irrigation was applied and by the 2nd of July when a second airborne image was acquired, the crop had recovered from water stress. The genetic variability of the different maize cultivars generated a gradient in their phenological stages of development, and consequently, there was variability in LAI values between the different plots. A fourth study site located in Zaragoza (Northern Spain, 41°46′ North, 1°37′ East) was used to conduct an intensive leaf sampling campaign to study the leaf optical properties of a peach orchard using an integrating sphere in the laboratory. The leaf optical properties of the leaves varied greatly due to nutrient stress conditions found in areas of the field.

2.2. Leaf-level measurements

Reflectance and transmittance measurements from leaves with different chlorophyll content and water stress levels were conducted to assess the influence of stress on the visible spectral region and, particularly, on the PRI index. In addition, optical variability of leaves enabled the estimation of the structural leaf parameter N (used in PROSPECT) required later for the modelling approach presented here (the complete experiment is described in Kempeneers et al., 2008). The instrument used was a Li-Cor 1800-12 integrating sphere (Li-Cor, Lincoln, NE, USA) coupled to a fibre optics spectrometer (Ocean Optics model USB2000 spectrometer, Ocean Optics, Dunedin, FL, USA). Reflectance and transmittance measurements of peach (Fig. 2a and b) and olive leaves (Fig. 2c and d) show variations in the visible spectral region due to nutrient and water stress levels affecting both chlorophyll and xanthophyll pigments.

During field campaigns, leaf reflectance measurements were also conducted in the study sites at the time of the flights with an ASD Field Spectrometer (FieldSpec Handheld Pro, ASD Inc., CO, USA) with a leaf clip probe. A total of 9 leaves per tree on 3 trees per treatment (olive and peach orchards) and 9 leaves per block on 6 blocks (maize) were measured in the field on each flight. Stem water potential measurements were conducted from the same sampled tree/blocks with a pressure chamber (Soil Moisture Equipment Corp. model 3000, Santa Barbara, CA, USA), and stomatal conductance was measured with a leaf porometer (model SC-1, Decagon Devices, Washington, DC, USA). In the olive tree site, a steady-state porometer was used to monitor stomatal conductance (model PMR-4, PP Systems, Hitchin Herts, UK).

2.3. Airborne imagery acquisition

A 6-band multispectral camera (MCA-6, Tetracam, Inc., California, USA) flying at 150 m above ground level (Berni et al, in press) was used to acquire imagery from the three study sites. The camera is built on 6 image sensors with 25 mm diameter bandpass filters of 10 nm FWHM (Andover Corporation, NH, USA). The image resolution is 1280×1024 pixels with 10-bit radiometric resolution and optic focal length of 8.5 mm, yielding an angular field-of-view (FOV) of 42.8°×34.7° and a spatial resolution of 15 cm at 150 m altitude. The bandsets used in each of the study sites comprised bands centered at 530 and 570 nm used to calculate the PRI index, as well as 550 nm, 670 nm, 700 nm and 800 nm bands to calculate TCARI/OSAVI index for chlorophyll content estimation (Haboudane et al., 2002), and NDVI for LAI estimation (Rouse et al., 1974).

Geometric calibration was performed using Bouguet's calibration (Bouguet, 2001) in order to recover the following intrinsic camera parameters: focal distance, principal point coordinates and lens radial distortion. The lens distortion model used was based on Wolf (1983), in which tangential and radial distortion are estimated, however in this case only the tangential distortion was taken into account (Berni et al., in press). Aerial triangulation was

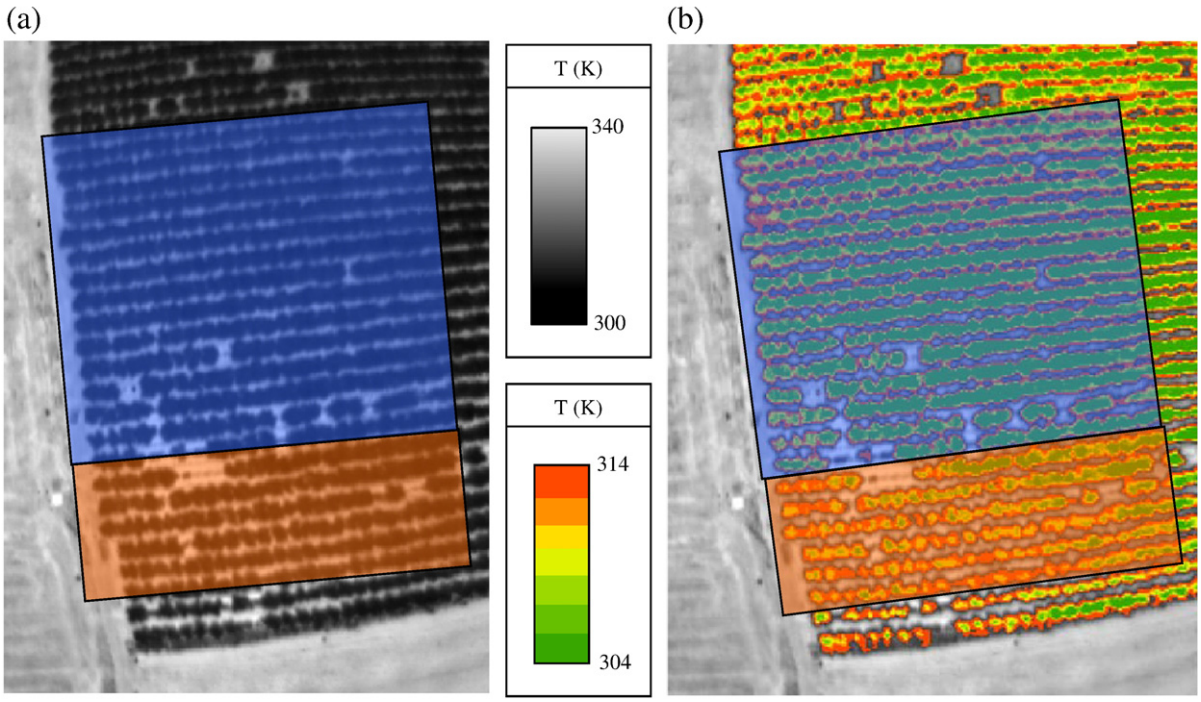

Fig. 3. (a) Imagery acquired with a thermal camera over the peach orchard where full irrigation (R) and deficit irrigation treatments (RDI) were applied; (b) Map of surface temperature of the experimental orchard.

Author's personal copy

used to georreference the multispectral images using Leica LPS (Leica Geosystems, Switzerland). Further correction was applied using the position of one of the cameras as reference and estimating the relative position of the other five by solving the system for each reference-camera pair. Images were calibrated to ground reflectance using the empirical line method with two reference targets (Smith & Milton, 1999). Two 4-square-meter black and white targets were leveled and placed in a central location of the flight path, measuring target reflectance with an ASD Field Spectrometer (FieldSpec Handheld Pro, ASD Inc., CO, USA) calibrated using a Spectralon panel (SRT-99-180, LabSphere, NH, USA). The empirical line method used to obtain surface reflectance from camera raw DN-values was validated in the study sites yielding a 1.17% RMSE (n=90) (Berni et al., in press). The *Photochemical Reflectance Index* (PRI) (Gamon et al., 1992), sensitive to the de-epoxidation state of the xanthophyll cycle pigments and used in previous studies to assess water stress (Suárez et al., 2008; Thenot et al., 2002), was calculated with the MCA-6 camera using two 10 nm FWHM filters centred at 530 and 570 nm wavelengths (Eq. (1)). Bands situated at 550, 670, 700 and 800 nm were used to calculate TCARI/OSAVI and NDVI indices using the Eqs. (2) and (3).

$$\mathrm{PRI} = \frac{R_{570} - R_{530}}{R_{570} + R_{530}} \tag{1}$$

$$\mathrm{TCARI/OSAVI} = \frac{3*[(R_{700} - R_{670}) - 0.2*(R_{700} - R_{550})*(R_{700}/R_{670})]}{(1+0.16)*(R_{800} - R_{670})/(R_{800} + R_{670} + 0.16)} \tag{2}$$

$$\mathrm{NDVI} = \frac{R_{800} - R_{670}}{R_{800} + R_{670}} \tag{3}$$

The thermal camera installed on board of the airborne platform was the Thermovision A40M (FLIR, USA), acquiring one image every 2 s during the flight. The image resolution was 320×240 pixels and 16 bits of at-sensor calibrated radiance with a 40° FOV lens, yielding 40 cm spatial resolution at 150 m altitude. The image sensor is a Focal Plane Array (FPA) based on uncooled microbolometers with a spectral range of 7.5–13 μm yielding calibrated radiance in the range 233–393 K. The camera was calibrated in the laboratory using a calibration

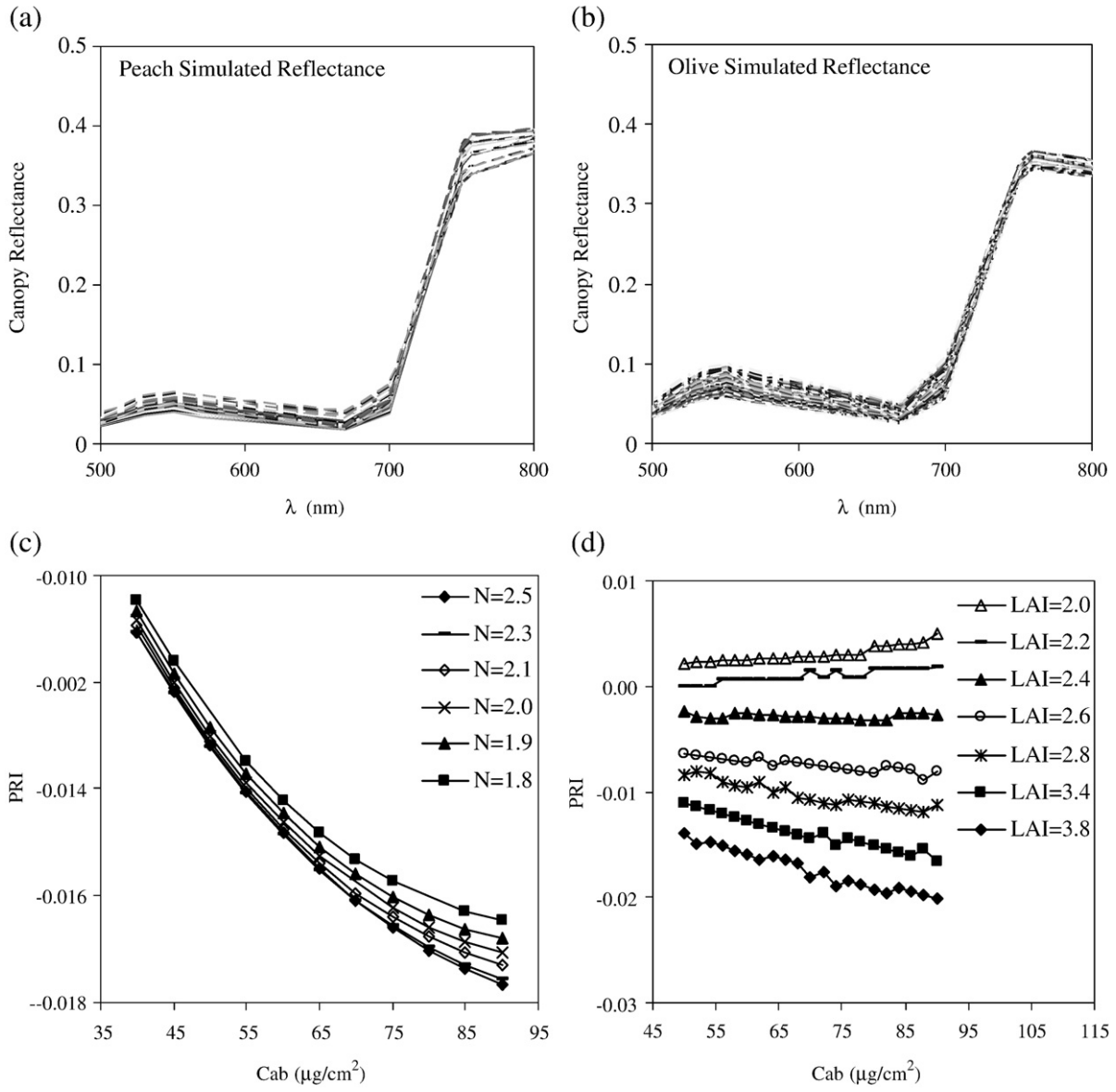

Fig. 4. Spectra used for modelling inversion for the peach orchard (a) and for the olive orchard (b). Relationship between chlorophyll content (Cab) and PRI for different N values (c), and for different LAI values (d).

Author's personal copy

Table 1
Nominal values and range of parameters used to construct the look-up tables for leaf and canopy modelling inversion with PROSPECT and FLIGHT models for the olive and peach orchard study sites

PROSPECT input parameters	Values/units used	
	Olive trees	Peach trees
N structural parameter	2.9	1.6
Cab (μg/cm^2)	50–90	50–72
Cm	0.025	0.015
Cw	0.025	0.015
Cs	0	0
FLIGHT input parameters	**Olive trees**	**Peach trees**
Leaf optical and structural parameters		
Hemispherical reflectance and transmittance of green leaves	PROSPECT	PROSPECT
Hemispherical reflectance and transmittance of senescent leaves	Not used	Not used
Leaf equivalent radius	0.007 m	0.02 m
Canopy layer and structural parameters		
Leaf Area Index of vegetation	2–4 m^2/m^2	1–2.6 m^2/m^2
Total scene Leaf Area Index	m^2/m^2	m^2/m^2
Fractional cover	0.32 m^2/m^2	0.22 m^2/m^2
Leaf Angle Distribution (LAD)	Empirical	Spherical
Fraction of green leaves	1	1
Fraction of senescent leaves	0	0
Fraction of bark	0	0
Hemispherical reflectance and transmittance of bark	Not used	Not used
Number of stands and position coordinates	Coord. (m)	Coord. (m)
Crown shape	Elliptical	Elliptical
Crown height and radius	m	m
Trunk height and radius	m	m
Background and viewing geometry		
Solar zenith and azimuth angles	Degrees	Degrees
Sensor zenith and azimuth angles	Degrees	Degrees
Soil reflectance	From image	From image
Soil roughness	0	0
Aerosol optical thickness (AOD)	0.15	0.15

Leaf structural parameters and leaf biochemical parameters were used for leaf-level simulation of reflectance and transmittance using PROSPECT. Canopy structural parameters were used as inputs in the FLIGHT model for simulating canopy reflectance by radiative transfer.

blackbody source (RAYBB400, Raytek, CA, USA), and switched on 1 h before flight until stable. Two internal calibrations are implemented in the sensor, a *non-uniformity correction* (NUC) and an internal temperature calibration. Atmospheric correction was needed to retrieve surface temperature, as described in Berni et al. (in press). *Single channel* atmospheric correction was conducted using the *Radiative Transfer Equation* (RTE), where the needed input parameters are atmospheric transmittance (τ_λ), emissivity (ε_λ), down-welling ($L^{\downarrow}_{atm,\lambda}$) and up-welling thermal radiation ($L^{\uparrow}_{atm,\lambda}$) which are driven mainly by water vapor content, air temperature and distance to object. The atmospheric calibration applied to the thermal images was validated in a specific campaign described in Berni et al. (in press) measuring simultaneously surface temperature with a thermal gun over 3 different surfaces: soil, white and black targets. The RMSE before calibration was 3.44 K, which was reduced down to 0.89 K after atmospheric correction. Fig. 3 shows a thermal image acquired over the peach orchard after conducting atmospheric correction (Fig. 3a) where differences between irrigated and water-stressed trees can be observed (Fig. 3b). Geometric calibration was conducted using the same methodology that was applied to the multispectral camera, but using resistive wires in the calibration pattern (Berni et al., in press). Exterior orientation, including camera position coordinates, pitch, roll and yaw, was acquired by the inertial navigation system onboard, allowing an initial estimate for the automated aerotriangulation. Sensor-to-ground distance across the image was calculated pixel by pixel, taking into account the effects of the camera's wide field of view and the airborne platform tilt angles. This distance was used to

Table 2
Nominal values and range of parameters used for leaf and canopy model inversion conducted with PROSPECT and SAILH for the corn study site

PROSPECT-SAILH input parameters	Values/units used
	Maize
Leaf optical and structural parameters	
N structural parameter	1.2–1.6
Cab (μg/cm^2)	5–100
Cm	0.0035
Cw	0.0015
Cs	0
Canopy layer and structural parameters	
Hot Spot size	0.01
Leaf Area Index	0.1–12
Leaf Angle Distribution (LAD)	Spherical
Background and viewing geometry	
Solar zenith and azimuth angles	Degrees
Soil reflectance	From image

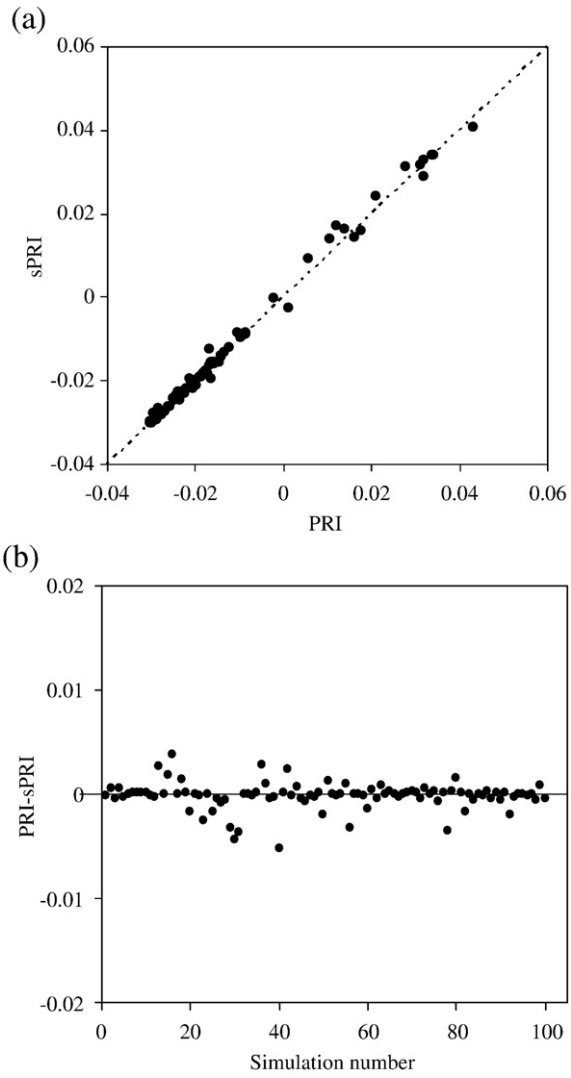

Fig. 5. Simulated PRI (sPRI) against airborne PRI (a), showing the PRI−sPRI differences(b).

Author's personal copy

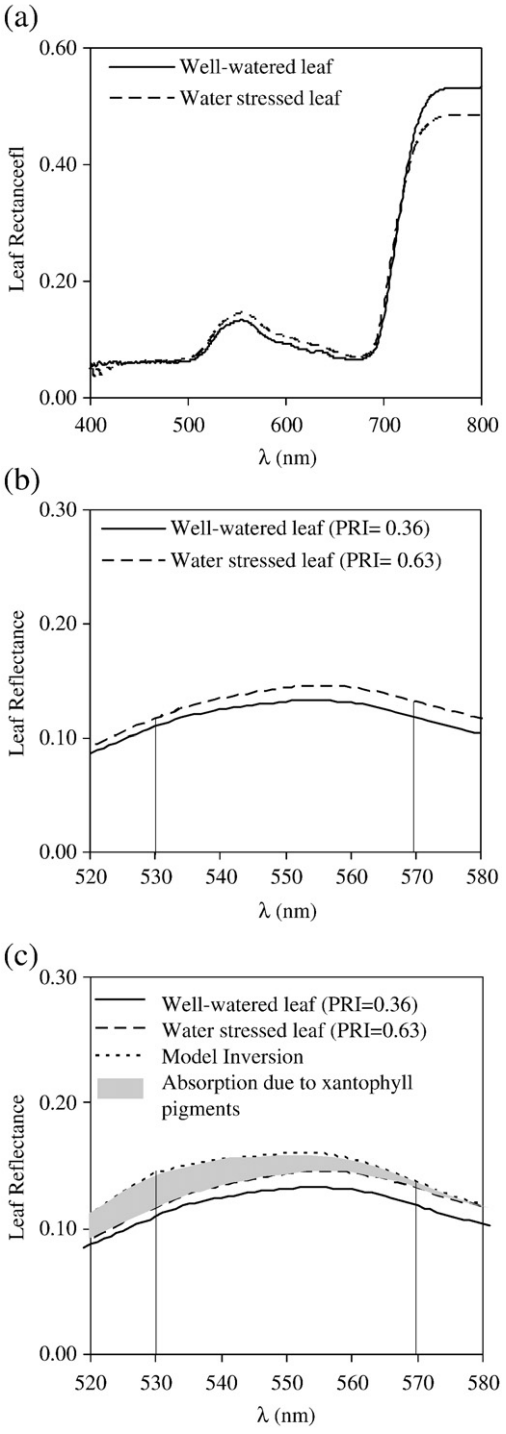

Fig. 6. (a) Peach leaf reflectance measured in the field for a stressed and an unstressed peach leaf. (b) Leaf spectra on the two wavelengths (530 and 570 nm) used to calculate the PRI index. (c) Leaf spectra on the PRI region and inverted spectra of the stressed leaf showing the effects of chlorophyll loss on leaf spectra and the effects of xanthophylls absorption.

generate a transmittance and thermal radiation map for an accurate calculation of surface temperature.

2.4. Radiative transfer modelling methods for simulating non-stress PRI

Radiative transfer simulations were conducted with PROSPECT (Jacquemoud & Baret, 1990) linked with SAILH model (Verhoef, 1984) for the maize field (a homogeneous canopy), and PROSPECT model linked to FLIGHT (North, 1996) for tree crops (olive and peach trees). The PROSPECT leaf optical properties model has been linked with several canopy reflectance models based on SAIL, such as GeoSAIL (Verhoef & Bach, 2003), 2M-SAIL (Weiss et al., 2001) or SAILH (hot spot effect added by Kuusk, 1991). An exhaustive review of models linked to PROSPECT (Jacquemoud et al., in press) include continuous crops (Bacour et al., 2002; Baret et al., 1995; Combal et al., 2002; Casa & Jones, 2004; González-Sanpedro et al., 2008; Jacquemoud et al., 1994, 1995, 2000; Koetz et al., 2005; Weiss et al., 2002; Yang & Ling, 2004; Zarco-Tejada et al., 2001), forestry areas (Le Maire et al., 2008; Meroni et al., 2004; Soudani et al., 2006; Zarco-Tejada et al., 2003, 2004; Zhang et al., 2005), and the global domain (Bacour et al., 2006; Baret et al., 2007; Trombetti et al., 2008; Weiss et al., 2007). In this study, the model PROSPECT was coupled to the SAILH model to simulate the canopy reflectance of the corn field under different irrigation treatments.

The 3-D *Forest Light Interaction Model*, (FLIGHT) is based on Monte Carlo ray tracing (MCRT) method as a tool to simulate the radiative transfer in a canopy structure (North, 1996). At the top of the canopy, the interaction of radiation within the vegetation depends on the contribution of several components such as leaves, stems, soil background, illumination and view properties of each canopy elements as well as on their number, area, orientation and location in space (Goel & Thompson, 2000; Koetz et al., 2005). FLIGHT radiative transfer model was previously used to simulate discontinuous canopy reflectance in conifer forests (Dawson et al., 1999; Koetz et al., 2004; Verrels et al., 2008) and in olive orchards (Suárez et al., 2008). In this work, the FLIGHT model was used together with PROSPECT to simulate peach and olive tree crown reflectance, specifically at 530

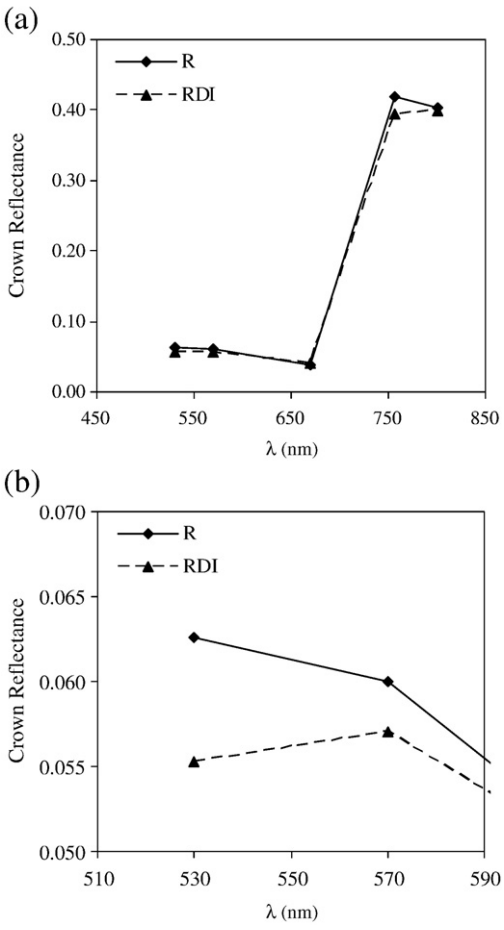

Fig. 7. Average crown reflectance derived from imagery of olive trees from the RDI and R treatments (a); spectra on the PRI region (b).

Author's personal copy

and 570 nm bands for effects of bidirectional reflectance distribution function (BRDF) on PRI simulation.

A sensitivity analysis was conducted to assess the influence of model input parameters on PRI bands, specifically leaf Cab and N, and canopy LAI (Fig. 4). The simulation conducted suggests that N and Cab leaf parameters, and the LAI canopy parameter are critical for simulating PRI at the canopy level. The suggested method consists on simulating a non-stress PRI value for a crop field (sPRI) by model inversion using the canopy reflectance from airborne imagery. The difference found between the image PRI (per tree or block level) and the non-stress simulated PRI by model inversion (sPRI), calculated as PRI−sPRI, would be associated with xanthophyll absorption levels at 530 nm.

The methodology applied for orchards through PROSPECT-FLIGHT model inversion was based on generating look-up tables independently for each crop and imagery conditions. The method consisted on targeting pure crowns under non-water-deficit conditions, and inverting the coupled leaf-canopy models for Cab and LAI. Model inversion was conducted fixing N (structural parameter), Cm (dry matter) and Cw (water content) values from the literature (Kempeneers et al., 2008, for peach trees; Zarco-Tejada et al., 2004 for olive trees). Cab and LAI were allowed to vary in the leaf- and canopy-level model inversion step, respectively. The rest of parameters were kept fixed, characterizing each crop field with inputs to represent the architecture of the orchard. The parameter ranges used to build the look-up tables are summarized in Table 1. The resulting simulated LUT spectra for olive and peach trees are presented in Fig. 4a and b.

For the corn study site, the parameters used for the coupled PROSPECT-SAILH model inversion are presented in Table 2. In this case, the parameters N and Cab at leaf level, and LAI at canopy level were inverted. The rest of the inputs were fixed to values and ranges found in literature for corn (Haboudane et al., 2004). Spectra were extracted from images acquired over the corn field for each of the 72 variety blocks. Block spectra were used as input for the model inversion, accounting for large within-field LAI differences found in the variety-trial study.

Simulated PRI obtained by model inversion for each crop field (sPRI) was compared with PRI extracted from the canopy reflectance for each pure crown/block. In addition, simulated PRI and image-extracted PRI from each orchard tree/corn block were compared against crown temperature and water potential measurements acquired at the time of each flight. The difference PRI−sPRI and the temperature for each corn block were assessed before and after irrigation for morning and afternoon flights, assessing the stress detection capabilities of the proposed methodology.

To demonstrate the successful simulation of PRI by model inversion (sPRI) using the airborne bandset for this study, one hundred synthetic spectra were randomly generated for N [1.2–1.6], Cab [5–90 μg/cm^2] and LAI [0.1–12] values. The bandset used for the simulation consisted on 5 bands located in the visible-NIR region at 530, 570, 670, 700 and 800 nm, bandset selected for the airborne camera to enable the calculation of PRI, TCARI/OSAVI, and NDVI. The rest of input values used are the ones presented in Table 2 for the corn study site. The input parameters Cab, LAI and N, and the PRI index

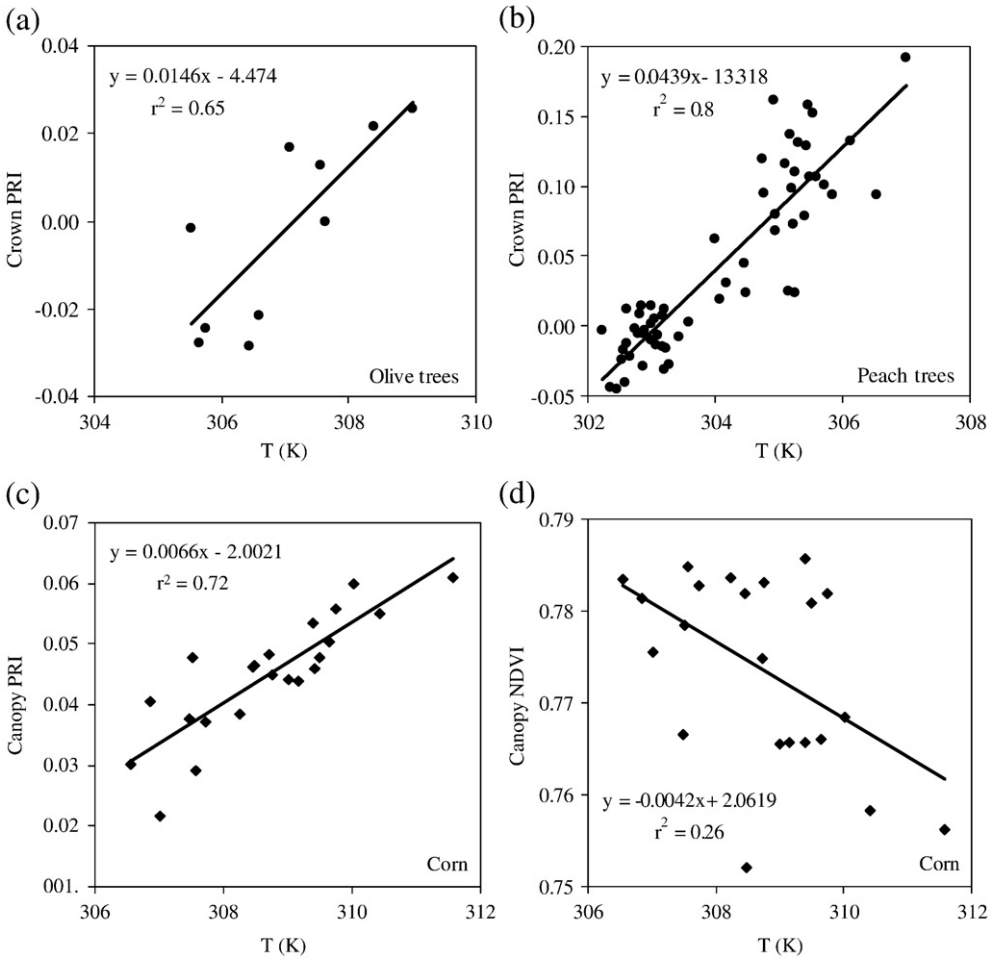

Fig. 8. Relationships obtained between crown/canopy PRI and vegetation surface temperatures derived from imagery for (a) olive trees; (b) peach trees; (c) corn, and (d) between canopy NDVI and temperature for corn.

Author's personal copy

were compared with the inversion outputs, yielding a RMSE of 5.45 μg/cm^2 (Cab), 1.1 (LAI), 0.13 (N). The results of this modelling approach confirm that PRI can be successfully simulated with 5-channel spectra (Fig. 5a), obtaining PRI−sPRI values close to 0 for a wide range of input Cab, N and LAI (Fig. 5b). The method proposed here based on using physical models, enabled the simulation of PRI for non-stress conditions accounting for N, Cab and LAI differences across the cropped field.

3. Results

3.1. PRI measurements at the leaf level

Leaf level measurements on olive and peach tree leaves showed differences in the leaf spectra between the full-irrigated (FI) and the regulated deficit irrigation (RDI) treatments. Fig. 6a shows the mean leaf spectra corresponding to both irrigation treatments. In the near infra-red part of the spectrum, differences can be detected due to leaf structural changes in response to water stress. Differences in the green region (Fig. 6b) are due to confounding effects of both chlorophyll content and xanthophyll absorption at 530 nm due to the water stress. To understand the confounding effects of chlorophyll absorption and the xanthophyll absorption, a modelling approach was undertaken. The PROSPECT radiative transfer model was used to invert the mean leaf spectrum measured under regulated deficit irrigation. Spectral differences found at 530 nm between the PROSPECT-simulated spectrum and the measured water-stress reflectance would correspond to xanthophyll pigment absorption (Fig. 6c).

3.2. PRI measurements at the canopy level

The mean spectrum corresponding to FI trees and RDI is shown in Fig. 7a. Differences due to water stress at 530 and 570 nm can be seen in Fig. 7b. The large differences at 530 nm between the two spectra are due to increased xanthophyll pigment absorption under water stress. At canopy scale, the relationship between PRI and temperature derived from the thermal airborne camera is shown in Fig. 8 for olive trees (Fig. 8a), for peach trees (Fig. 8b), and for maize (Fig. 8c). For olive and peach trees, pure crown PRI was calculated from airborne imagery and related to surface temperature estimated from the airborne thermal imagery. Canopy temperature (T) was related to PRI, coefficients of determination of the regression lines of PRI against T yielded r^2=0.65 for the olive trees, and r^2=0.8 for the peach trees. For the same set of peach trees the determination coefficient of the relationship of airborne-derived temperature with TCARI/OSAVI index at canopy scale yielded 0.0017, demonstrating that PRI correlation with T was not due to differences in Chlorophyll content. The analysis on the maize field was conducted at block scale with PRI and T calculated for each of the 72 experimental blocks in the field. The relationship shown (Fig. 8c) corresponds to a set of blocks with similar NDVI, therefore avoiding structural effects on the PRI vs. T relationship. The determination coefficient for that relationship (r^2=0.72) illustrates the consistency of PRI as an indicator of water stress in maize under equal structural conditions. For the same set of blocks with similar NDVI, the relationship between NDVI and canopy temperature (Fig. 8d), yielded a low coefficient of determination (r^2=0.26), demonstrating that structure was not the driver between

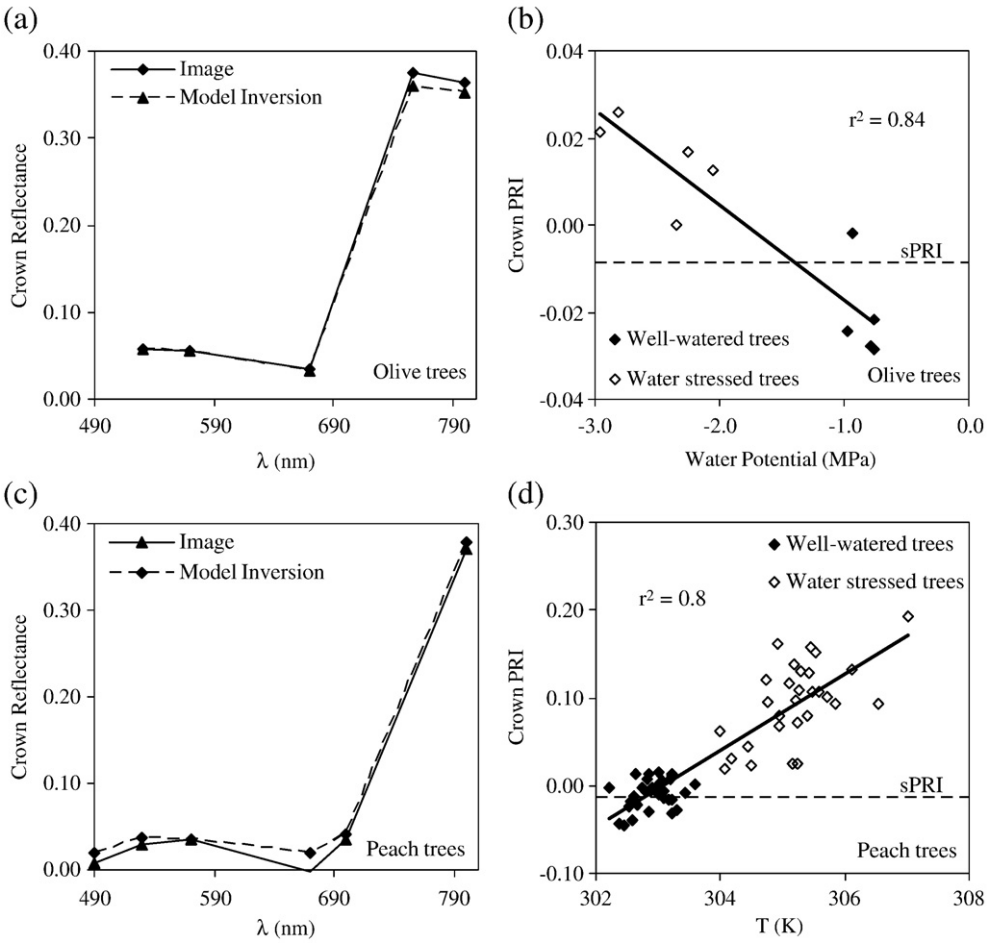

Fig. 9. Comparison between mean full-irrigated crown spectrum and the inverted modelled spectrum for (a) olive, and (c) peach trees. Relationship between PRI and water potential for (b) olive trees, and (d) PRI with temperature for peach trees. The relative position of individual crown PRI as compared with the calculated PRI from the theoretical spectrum is shown.

Author's personal copy

PRI and canopy T relationship. In the three study sites, peach, olive orchards and maize field, airborne canopy PRI values for water stressed trees/blocks were higher than the PRI values from fully irrigated vegetation.

3.3. Assessing stress with PRI through model inversion

A PROSPECT-FLIGHT model inversion method was conducted using the mean spectra extracted from the airborne imagery for the olive and the peach orchards. Fig. 9a and c shows the image spectra used for the inversion for olive and peach trees, respectively, along with canopy reflectance obtained by model inversion. PRI values corresponding to the inverted spectra (Fig. 9b and d) used as the theoretical PRI for non-stress conditions (sPRI) are shown along with the PRI values extracted from pure crowns on both orchards. The crown PRI values for full and deficit irrigation are compared against the theoretical PRI (sPRI) for non-stress conditions (Fig. 9b and d). Results show that PRI for RDI trees are higher than simulated non-stress PRI

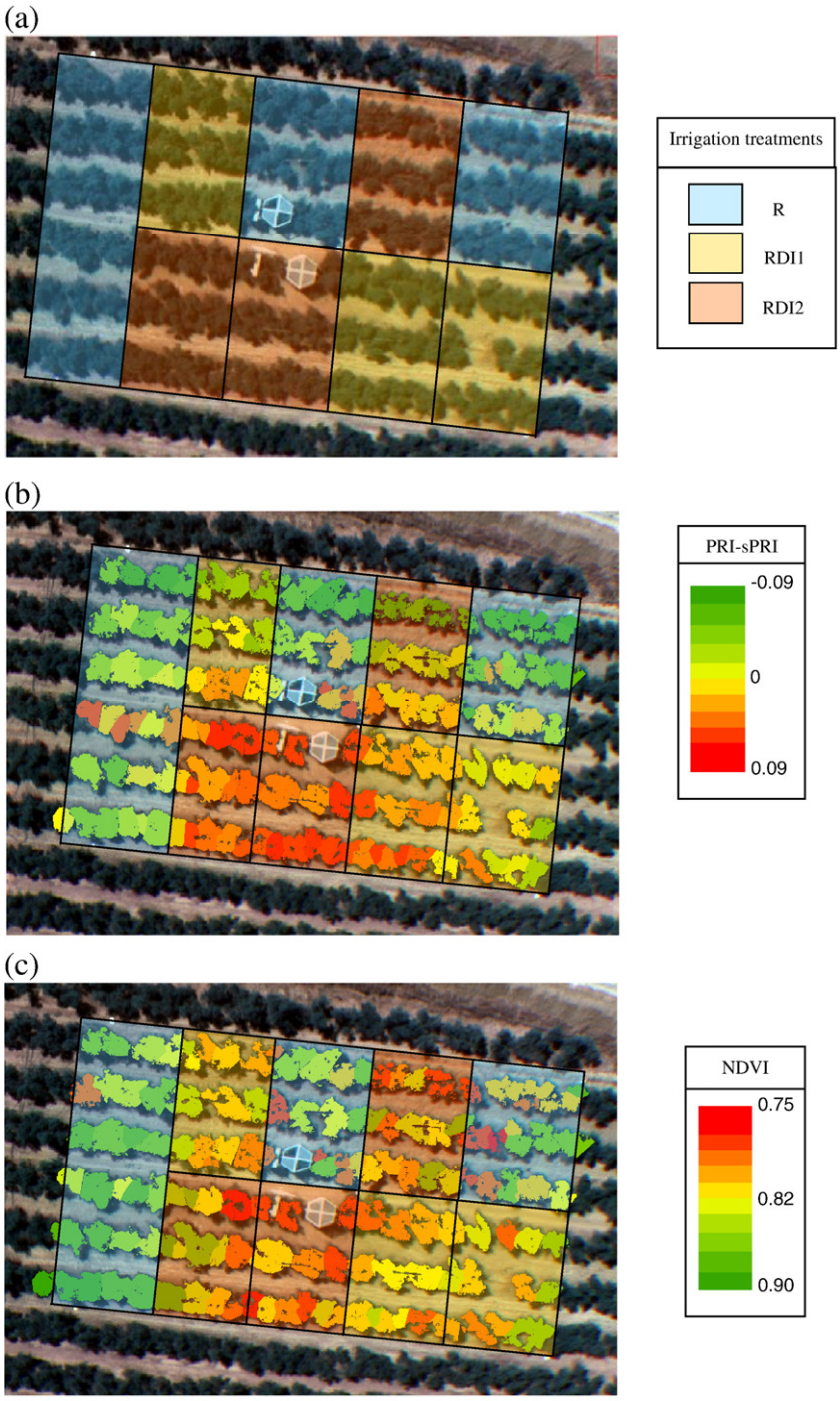

Fig. 10. (a) Overview of the olive orchard experiment with three irrigation treatments applied; (b) crown PRI minus simulated PRI (PRI − sPRI) map of the experiment; (c) crown NDVI map.

Author's personal copy

for both olive and peach trees. On the contrary, all FI trees show PRI values around or below the simulated PRI value for non-stress conditions. Consistently, RDI trees showed higher PRI values than the simulated non-stress PRI values derived from model inversion. This method enables an operational detection of stressed trees using the modelling approach to account for LAI and chlorophyll content effects on modelled PRI index values. A map was generated representing the distance PRI−sPRI as an indicator of water stress for the olive orchard (Fig. 10a). The map shows the spatial distribution of water stress as a function of irrigation levels (Fig. 10b). Positive values of PRI−sPRI (red color) indicate water stress, while negative values (green color) indicate non-stress conditions. The PRI−sPRI map clearly shows that water-stress is detected in trees of the RDI1 and RDI2 treatments (Fig. 10a), while the FI treatments are well identified as control. The spatial variability of canopy leaf area index through the normalized difference vegetation index (NDVI) (Fig. 10c) was assessed. The NDVI map, on the contrary, did not detect water stress levels as well as the PRI−sPRI indicator did. These results demonstrate that a physiological index such as PRI, when modelled to account for leaf and canopy inputs N, Cab and LAI, was superior to NDVI to detect within-field water stress variability.

In the maize study site, the mean field pure-vegetation spectrum was inverted using the coupled PROSPECT-SAILH model. The inversion method was conducted on each of the four images acquired in this study, consisting on pre- and post-irrigation dates at 10.00–11.00 GMT (morning) and 13.00–14.00 GMT (midday). Two images were acquired under water deficit conditions in the morning and at midday of June 6th. Another two images were acquired after irrigation was applied on July 2nd in the morning and at midday. After conducting the model inversion for the four conditions, simulated non-stress PRI (sPRI) was calculated and compared to each block PRI value extracted from the imagery. Block PRI values are shown against the simulated non-stress PRI baseline (sPRI) for the maize field (Fig. 11a to d). Before irrigation, on the 6th of June (Fig. 11a and c) block PRI values were located below or around the theoretical non-stress sPRI baseline in the morning (10:10 GMT). At midday (14:20 GMT), on the contrary, airborne PRI values were located over the theoretical sPRI baseline, suggesting that the blocks are under stress conditions (Fig. 11c). After irrigation, on the 2nd of July, airborne PRI values were around or below the theoretical non-stress sPRI obtained by PROSPECT-SAILH inversion, both in the morning (11:03 GMT; Fig. 11b) and also at midday (13:11 GMT; Fig. 11d). These results suggest that this methodology is capable of detecting water stress in continuous crop canopies such as maize, being able to assess the response to irrigation with the PRI index when modelled for N, Cab and LAI effects.

A second modelling approach was undertaken to deal with crop canopy structural effects for each maize block extracted from the reflectance imagery. Each block reflectance extracted from the airborne imagery was used as input for model inversion, obtaining the non-stress PRI value for each maize block (sPRI). For each of the 72 blocks extracted from the image, the difference PRI−sPRI was calculated. Block PRI−sPRI along with block canopy temperature minus air temperature (Tc−Ta) are shown in Fig. 12 for pre- and post-irrigation in the morning and midday. On the 6th of June, before irrigation, values for PRI−sPRI and Tc−Ta at 10:10 GMT and at 14:20 GMT are shown in Fig. 12a and c. The mean Tc−Ta values

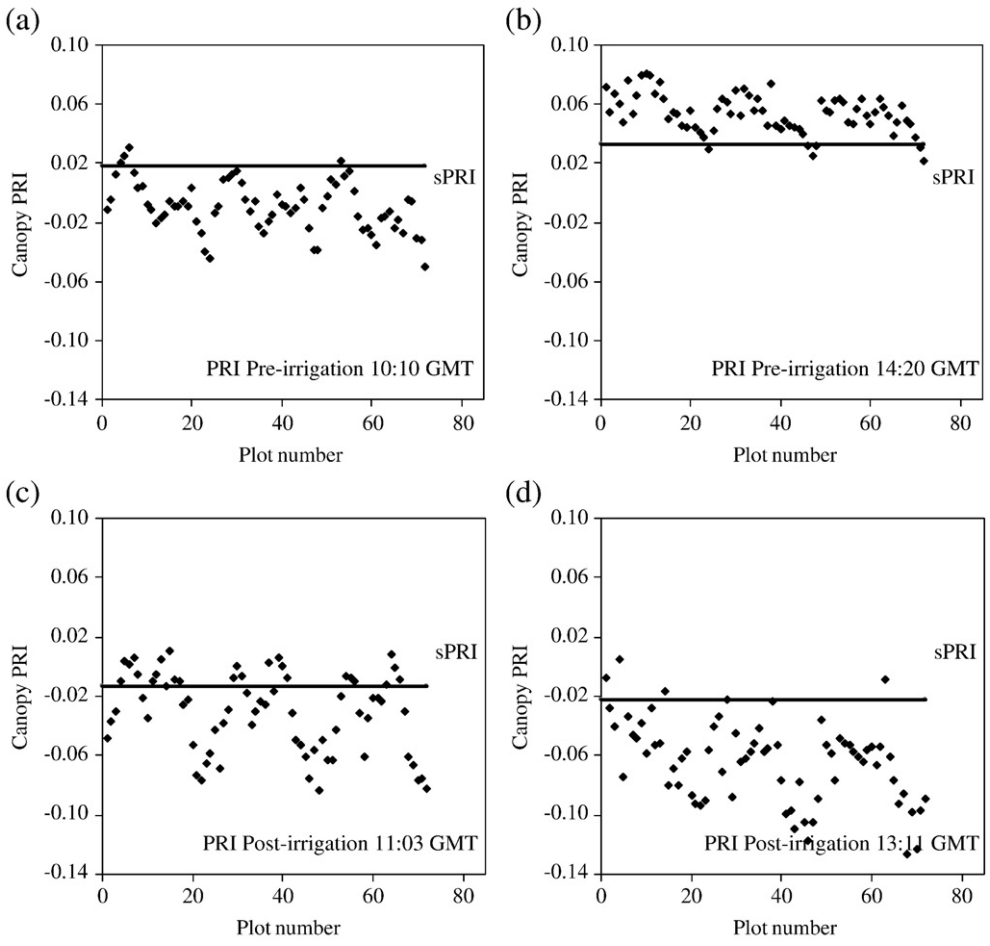

Fig. 11. Corn PRI values compared with the simulated PRI values (sPRI), calculated before irrigation for the morning (a), at midday (b), and after irrigation, in the morning (c) and at midday (d).

Author's personal copy

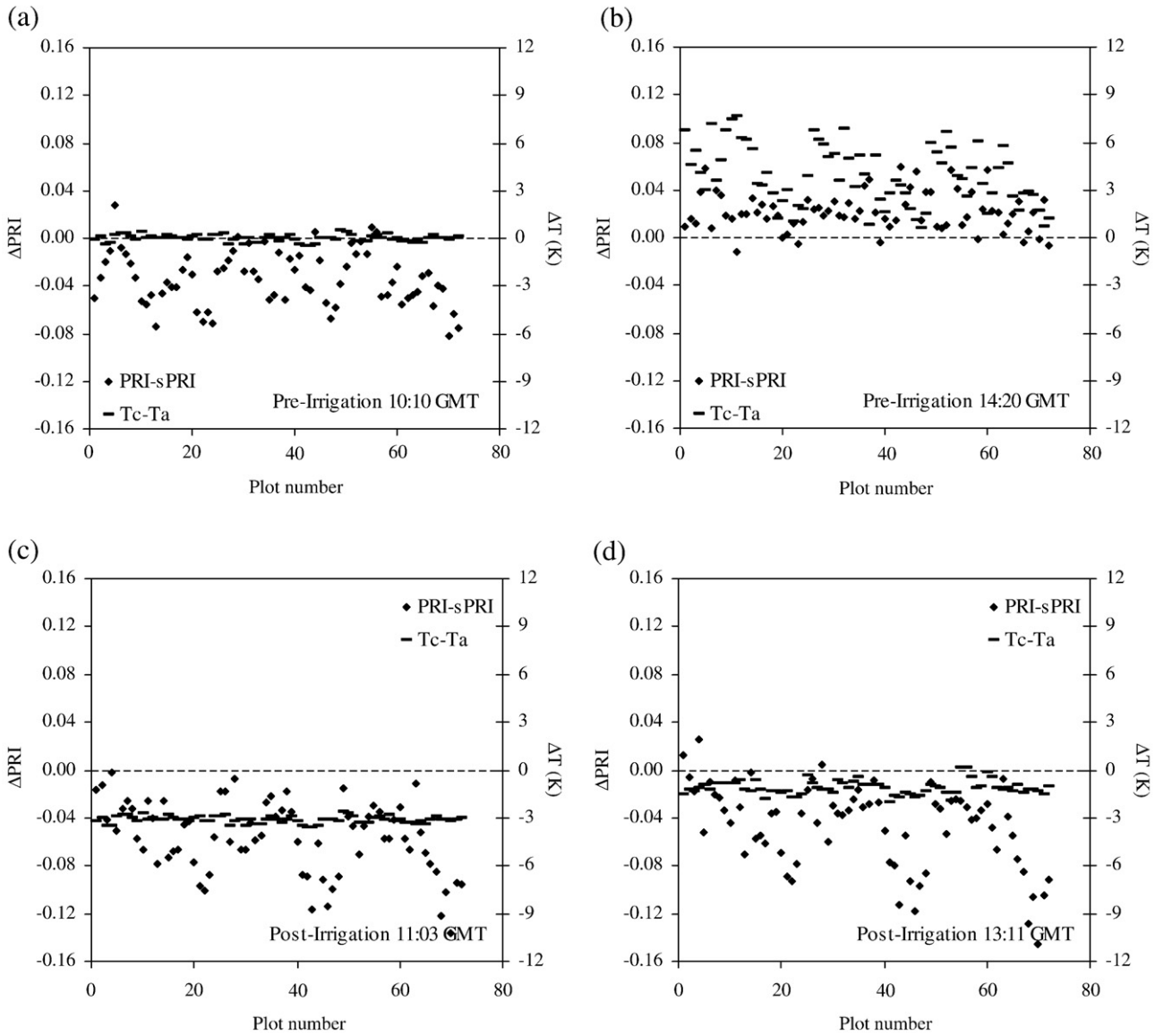

Fig. 12. Corn block PRI−sPRI (diamonds) and block surface temperature minus air temperature (Tc−Ta; dashes) in the morning and midday before irrigation (a and b respectively) and after irrigation (c and d).

obtained in the morning prior to irrigation was −0.02 K, rising up to 3.87 K at midday, with higher stress conditions. Airborne Tc−Ta values were consistent with the PRI−sPRI values, PRI−sPRI and Tc−Ta values showed a wide range of variability. Such high variability suggests the different cultivars responded differently to water deprivation, as Tc−Ta differences were up to 8 K. The same variability is obtained in PRI−sPRI values as compared with Tc−Ta variability, concluding that this methodology could be useful for screening different cultivars in their response to water deficits. Results on the data acquired after irrigation (on the 2nd of July) are shown in Fig. 12b and d. Again, Tc−Ta values are lower (yielding an average value of −3.13 K in the morning and −1.13 K at midday), being consistent with PRI−sPRI values around zero, showing that airborne PRI values are close to the simulated non-stress PRI values as the crop is recovered from water stress. Fig. 13a to d shows PRI−sPRI maps, observing that maize fields under stress conditions before irrigation do not present stress symptoms in the morning (Fig. 13a), while high PRI−sPRI values showed significant stress at midday. After irrigation, maize blocks did not show stress in the morning (Fig. 13c), while slightly higher PRI−sPRI differences were found at midday (Fig. 13d), as higher evaporative demand exists. Consistently, Fig. 13 demonstrates that the highest stress conditions were detected at midday by the PRI−sPRI indicator before irrigation.

4. Conclusions

This study presents a methodology for water stress detection in annual and perennial irrigated crops using remotely sensed PRI index and radiative transfer modelling. The method accounts for leaf and canopy inputs N, Cab and LAI to simulate the PRI values to identify crop crowns/blocks under stress. The methodology presented was successfully tested on two tree orchards (olive and peach trees) and a closed canopy of an annual crop (maize). The PRI index tracked water stress levels in crops under deficit irrigation, and yielded robust relationships against canopy temperatures (r^2=0.65 for olive trees, r^2=0.8 for peach trees, and r^2=0.72 for maize). Moreover, within-field structural effects on PRI were assessed, demonstrating that PRI was successfully related with canopy temperature (r^2=0.72) for crop blocks under same NDVI values, thus showing that PRI is sensitive to water stress conditions independently of canopy structural effects. In addition, the lack of relationship between crown temperature and TCARI/OSAVI for peach trees (r^2=0.0017) demonstrates PRI is not

Author's personal copy

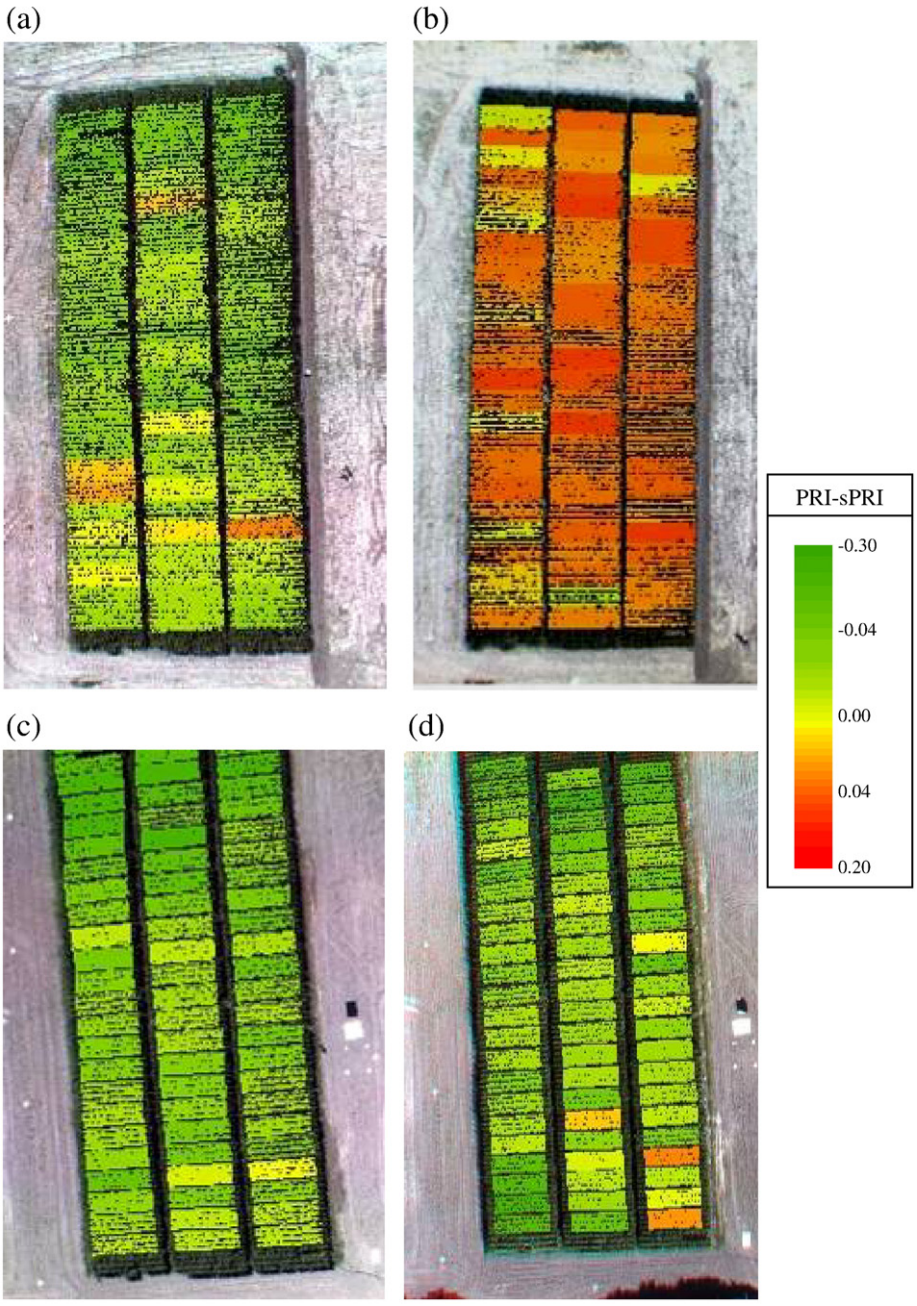

Fig. 13. Corn PRI minus block simulated PRI (PRI−sPRI) for the four image acquisitions before irrigation ((a) in the morning and (b) at midday), and after irrigation in the morning (c) and midday (d).

driven by differences in chlorophyll content. The ability of PRI to detect water stress before vegetation structure is affected is critical as a pre-visual indicator of stress. However, PRI was highly affected by both background and canopy structure, requiring correct modelling methods for successful mapping of water stress and its spatial variability. Modelling inversion methods enabled accounting for background and crop/orchard characteristics independently for each crop field and imagery acquired with the airborne multi-spectral sensor. Two different canopy radiative transfer models were used depending on the crop structure, SAILH for maize crop and FLIGHT model for tree orchards (olive and peach trees), while simulations at leaf scale were conducted successfully with the PROSPECT leaf model.

Results demonstrated that airborne canopy PRI values higher than the theoretical non-stress PRI, when accounting for N, Cab and LAI via radiative transfer models, correspond to vegetation pixels under water stress. Consistency was found in three crops where this methodology was applied. Airborne PRI values compared with the theoretical non-stress PRI, calculated as PRI−sPRI, agreed in amplitude with the irrigation levels applied, and the stress level before and after irrigation. The results obtained in this study demonstrate that PRI is a pre-visual indicator of water stress, i.e., when no effects could be detected visually, and it can be modelled for estimating non-stress thresholds to be used for stress-detection. Finally, this methodology based on a narrow-band index derived from the visible part of the spectrum may be potentially used as an alternative to thermal imagery for assessing water stress. High-resolution thermal imagers are generally more expensive and their availability more limited than CCD/CMOS instruments onboard airborne and potential satellite platforms.

Author's personal copy

Acknowledgments

Financial support from the Spanish Ministry of Science and Innovation (MCI) for the projects AGL2005-04049, EXPLORA-INGENIO AGL2006-26038-E/AGR, CONSOLIDER CSD2006-67, and AGL2003-01468 is gratefully acknowledged, and in-kind support provided by Bioiberica through the project PETRI PET2005-0616. Technical support from UAV Navigation and Tetracam Inc. is also acknowledged. M. Morales, C. Ruz, G. Sepulcre-Cantó, D. Notario, M. Guillén, C. Trapero, I. Calatrava, A. Vera and M. Ruiz Bernier are acknowledged for measurements and technical support in field and airborne campaigns.

References

Asner, G. P., Carlson, K. M., & Martin, R. E. (2005). Substrate age and precipitation effects on Hawaiian forest canopies from spaceborne imaging spectroscopy. *Remote Sensing of Environment*, *98*, 457–467.

Bacour, C., Baret, F., Béal, D., Weiss, M., & Pavageau, K. (2006). Neural network estimation of LAI, fAPAR, fCover and LAI×Cab, from top of canopy MERIS reflectance data: Principles and validation. *Remote Sensing of Environment*, *105*, 313–325.

Bacour, C., Jacquemoud, S., Leroy, M., Hautecoeur, O., Weiss, M., Prévot, L., Bruguier, N., & Chauki, H. (2002). Reliability of the estimation of vegetation characteristics by inversion of three canopy reflectance models on airborne POLDER data. *Agronomie: Agriculture and Environment*, *22*, 555–565.

Baret, F., Clevers, J. P. W., & Steven, M. D. (1995). The robustness of canopy gap fraction estimates from red and near-infrared reflectances: A comparison of approaches. *Remote Sensing of Environment*, *54*, 141–151.

Baret, F., Hagolle, O., Geiger, B., Bicheron, P., Miras, B., Huc, M., Berthelot, B., Fernando Niño, F., Weiss, M., Samain, O., Roujean, J. L., & Leroy, M. (2007). LAI, fAPAR and fCover CYCLOPES global products derived from VEGETATION Part 1: Principles of the algorithm. *Remote Sensing of Environment*, *110*(3), 275–286.

Barton, C. V. M., & North, P. R. J. (2001). Remote sensing of canopy light use efficiency using the Photochemical Reflectance Index. Model and analysis. *Remote Sensing of Environment*, *78*(264), 273.

Berni J.A.J., Zarco-Tejada P.J., Suarez L., Fereres E., (in press) Thermal and narrow-band multispectral remote sensing for vegetation monitoring from an unmanned aerial vehicle. *IEEE Transactions on Geoscience and Remote Sensing*, October, 2008.

Bouguet, J. (2001). *Camera Calibration Toolbox for Matlab.* (http://www.vision.caltech.edu/bouguetj/calibdoc/index.html).

Casa, R., & Jones, H. G. (2004). Retrieval of crop canopy properties: a comparison between model inversion from hyperspectral data and image classification. *International Journal of Remote Sensing*, *25*, 1119–1130.

Chalmers, D. J., Mitchell, P. D., & van Heek, L. (1981). Control of peach tree growth and productivity by regulated water supply, tree density and summer pruning. *Journal of the American Society for Horticultural Science*, *106*, 307–312.

Cohen, Y., Alchanatis, V., Meron, M., Saranga, Y., & Tsipris, J. (2005). Estimation of leaf potential by thermal imagery and spatial analysis. *Journal of Experimental Botany*, *56*, 1843–1852.

Combal, B., Baret, F., & Weiss, M. (2002). Improving canopy variables estimation from remote sensing data by exploiting ancillary information. Case study on sugar beet canopies. *Agronomie*, *22*, 205–215.

Dawson, T. P., Curran, P. J., North, P. R. J., & Plummer, S. E. (1999). The propagation of foliar biochemical absorption features in forest canopy reflectance: A theoretical analysis. *Remote Sensing of Environment*, *67*(2), 147–159.

Dobrowsky, S. Z., Pushnik, J. C., Zarco-Tejada, P. J., & Ustin, S. L. (2005). Simple reflectance indices track heat and water stress-induced changes in steady-state chlorophyll fluorescence at the canopy scale. *Remote Sensing of Environment*, *97*, 403–414.

Drolet, G. G., Huemmrich, K. F., Hall, F. G., Middleton, E. M., Black, T. A., Barr, A. G., & Margolis, H. A. (2005). A MODIS-derived Photochemical Reflectance Index to detect inter-annual variations in the photosynthetic light-use efficiency of a boreal deciduous forest. *Remote Sensing of Environment*, *98*, 212–224.

Evain, S., Flexas, J., & Moya, I. (2004). A new instrument for passive remote sensing: 2. Measurement of leaf and canopy reflectance changes at 531 nm and their relationship with photosynthesis and chlorophyll fluorescence. *Remote Sensing of Environment*, *91*, 175–185.

Fereres, E., & Soriano, M. (2007). Deficit irrigation for reducing agricultural water use. *Journal of Experimental Botany*, *Vol. 58*, 147–159.

Fuentes, D. A., Gamon, J. A., Cheng, Y., Claudio, H. C., Qiu, H. L., Mao, Z., Sims, D. A., Rahman, A. F., Oechel, W., & Luo, H. (2006). Mapping carbon and water vapour fluxes in a chaparral ecosystem using vegetation indices derived from AVIRIS. *Remote Sensing of Environment*, *103*, 312–323.

Gamon, J. A., Peñuelas, J., & Field, C. B. (1992). A narrow-wave band spectral index that track diurnal changes in photosynthetic efficiency. *Remote Sensing of Environment*, *41*, 35–44.

Goel, N. S., & Thompson, R. L. (2000). A snapshot of canopy reflectance models and a universal nodel for the radiation regime. *Remote Sensing Reviews*, *18*(2), 197–225.

González-Sanpedro, M. C., Le Toan, T., Moreno, J., Kergoat, L., & Rubio, E. (2008). Seasonal variations of leaf area index of agricultural fields retrieved from Landsat data. *Remote Sensing of Environment*, *112*(3), 810–824.

Guo, J., & Trotter, C. M. (2004). Estimating photosynthetic light-use efficiency using the Photochemical Reflectance Index: Variations among species. *Functional Plant Biology*, *31*, 255–565.

Haboudane, D., Miller, J. R., Pattey, E., Zarco-Tejada, P. J., & Strachan, I. (2004). Hyperspectral vegetation indices and novel algorithms for predicting green LAI of crop canopies: Modeling and validation in the context of precision agriculture. *Remote Sensing of Environment*, *90*(3), 337–352.

Haboudane, D., Miller, J. R., Tremblay, N., Zarco-Tejada, P. J., & Dextraze, L. (2002). Integrated narrow-band vegetation indices for prediction of crop chlorophyll content for application to precision agriculture. *Remote Sensing of Environment*, *84* (2–3), 416–426.

Hsiao T. C., Bradford K. J. 1983. *Physiological consequences of cellular water deficits*. In: Taylor H.M., Jordan W.R., Sinclair T.R., eds. Limitations to efficient water use in crop production. Madison, WI: ASA, CSSA, SSSA, 227–265.

Hsiao, T. C., Fereres, E., Acevedo, E., & Henderson, D. W. (1976). *Water stress and dynamics of growth and yield of crops*. Water and plant life: Problems and modern approaches : Springer.

Idso, S. B., Jackson, R. D., Pinter, P. J., Reginato, R. J., & Hatfield, J. L. (1981). Normalizing the stress-degree-day parameter for environmental variability. *Agricultural and Forest Meteorology*, *24*, 45–55.

Idso, S. B., Jackson, R. D., & Reginato, R. J. (1978). Extending the "degree day" concept of phenomenological development to include water stress effects. *Ecology*, *59*, 431–433.

Jackson, R. D., Idso, S. B., Reginato, R. J., & Ehrier, W. L. (1977). Crop temperature reveals stress. *Crop Soils*, *29*, 10–13.

Jackson, R. D., Idso, S. B., Reginato, R. J., & Pinter, P. J. (1981). Canopy temperature as a crop water-stress indicator. *Water Resources Research*, *Vol. 17*, 1133–1138.

Jackson, R. D., & Pinter, P. J., Jr. (1981). Detection of water stress in wheat by measurement of reflected solar and emitted thermal IR radiation. *Spectral signatures of objects in remote sensing, Institut National de la Reserche Agronomique, Versalles, France* (pp. 399–406).

Jacquemoud, S., & Baret, F. (1990). PROSPECT: A model of leaf optical properties spectra. *Remote Sensing of Environment*, *34*, 75–91.

Jacquemoud, S., Baret, F., Andrieu, B., Danson, F. M., & Jaggard, K. (1995). Extraction of vegetation biophysical parameters by inversion of the PROSPECT + SAIL model on sugar beet canopy reflectance data — Application to TM and AVIRIS sensors. *Remote Sensing of Environment*, *52*, 163–172.

Jacquemoud, S., Bacour, C., Poilve, H., & Frangi, J. -P. (2000). Comparison of four radiative transfer models to simulate plant canopies reflectance — Direct and inverse mode. *Remote Sensing of Environment*, *74*, 471–481.

Jacquemoud, S., Flasse, S., Verdebout, J., & Schmuck, G. (1994). Comparison of several optimization methods to extract canopy biophysical parameters. *Proc. 6th international symposium on physical measurements and signatures in remote sensing, Val d'Isère (France), 17–21 January 1994* (pp. 291–298). CNES.

Jacquemoud S., Verhoef W., Baret W., Bacour C., Zarco-Tejada P.J., Asner G.P., François C., Ustin S.L., (in press) PROSPECT+SAIL: 16 years of use for vegetation characterization. *Remote Sensing of Environment* (February 2008).

Kempeneers, P., Zarco-Tejada, P. J., North, P. R. J., De Backer, S., Delalieux, S., Sepulcre-Cantó, G., Morales, F., et al. (2008). Model inversion for chlorophyll estimation in open canopies from hyperspectral imagery. *International Journal of Remote Sensing*, *29*(17–18), 5093–5111 (September 2008).

Koetz, B., Baret, F., Poilvé, H., & Hill, J. (2005). Use of coupled canopy structure dynamic and radiative transfer models to estimate biophysical canopy characteristics. *Remote Sensing of Environment*, *95*(1), 115–124.

Koetz, B., Schaepman, M., Morsdorf, F., Bowyer, P., Itten, K., & Allgöwer, B. (2004). Radiative transfer modeling within heterogeneous canopy for estimation of forest fire fuel properties. *Remote Sensing of Environment*, *92*, 332–344.

Kuusk, A. (1991). The hot spot effect in plant canopy reflectance. In R. B. Myneni, & J. Ross (Eds.), *Photon-vegetation interactions. Applications in optical remote sensing and plant ecology* (pp. 139–159). Berlin: Springer Verlag.

Leinonen, I., & Jones, H. G. (2004). Combining thermal and visible imagery for stimulating canopy temperature and identifying plant stress. *Journal of Experimental Botany*, *55*, 1423–1431.

Le Maire, G., François, C., Soudani, K., Berveiller, D., Pontailler, J. Y., Bréda, N., et al. (2008). Calibration and validation of hyperspectral indices for the estimation of biochemical and biophysical parameters of broadleaves forest canopies. *Remote Sensing of Environment*, *112*(10), 3846–3864.

Meroni, M., Colombo, R., & Panigada, C. (2004). Inversion of a radiative transfer model with hyperspectral observations for LAI mapping in poplar plantations. *Remote Sensing of Environment*, *92*, 195–206.

Möller, M., Alchanatis, V., Cohen, Y., Meron, M., Tsipris, J., Naor, A., Ostrovsky, V., Sprintsin, M., & Cohen, S. (2007). Use of thermal and visible imagery for estimating crop water status of irrigated grapevine. *Journal of Experimental Botany*, *Vol. 58*(4), 827–838.

Nakaji, T., Oguma, H., & Fujinuma, Y. (2006). *International Journal of Remote Sensing*, *27* (3), 493–509.

Nichol, C. J., Huemmrich, K. F., Black, T. A., Jarvis, P. G., Walthall, J. G., & Hall, F. G. (2000). Remote sensing of photosynthetic-light-use efficiency of boreal forest. *Agricultural and Forest Meteorology*, *101*, 131–142.

Nichol, C. J., Lloyd, J., Shibistova, O., Arneth, A., Röser, C., Knohl, A., Matsubara, S., & Grace, J. (2002). Remote sensing of photosynthetic-light-use-efficiency of a Siberian boreal forest. *Tellus*, *54B*, 677–687.

Nichol, C. J., Rascher, U., Matsubara, S., & Osmond, B. (2006). Assessing photosynthetic efficiency in an experimental mangrove canopy using remote sensing and chlorophyll fluorescence. *Trees*, *20*, 9–15.

North, P. R. J. (1996). Three-dimensional forest light interaction model using a montecarlo method. *IEEE Transactions on Geosciences and Remote Sensing*, *34*(5), 946–956.

Author's personal copy

Peguero-Pina, J. J., Morales, F., Flexas, J., Gil-Pelegrín, E., & Moya, I. (2008). Photochemistry, remotely sensed physiological reflectance index and de-epoxidation state of xanthophyll cycle in *Quercus coccifera* under intense drought. *Oecologia*, *156*(1), 1–11.

Pérez-Priego, O., Zarco-Tejada, P. J., Sepulcre-Cantó, G., Miller, J. R., & Fereres, E. (2005). Detection of water stress in orchard trees with a high-resolution spectrometer through chlorophyll fluorescence in-filling of the O_2-A band. *IEEE Transactions on Geoscience and Remote Sensing*, *43*, 2860–2869.

Rouse J.W., Haas R.H., Schell J.A., Deering D.W. & Harlan J.C., (1974). Monitoring the vernal advancements and retrogradation of natural vegetation in Nasa/Gsfc final report (ed. MD, U.G.) p. 371.

Sepulcre-Cantó, G., Zarco-Tejada, P. J., Jiménez-Muñoz, J. C., Sobrino, J. A., de Miguel, E., & Villalobos, F. J. (2006). Within-field thermal variability detection as function of water stress in *Olea europaea* L. orchards with high spatial remote sensing imagery. *Agricultural and Forest Meteorology*, *136*, 31–44.

Sepulcre-Cantó, G., Zarco-Tejada, P. J., Jiménez-Muñoz, J. C., Sobrino, J. A., Soriano, M. A., Fereres, E., Vega, V., & Pastor, M. (2007). Monitoring yield and fruit quality parameters in open-canopy tree crops under water stress. Implications for ASTER. *Remote Sensing of Environment*, *107*, 455–470.

Sepulcre-Cantó G., Zarco-Tejada P.J., Sobrino J.A., Berni J.A.J., Jiménez Muñoz J.C., Gastellu-Etchegorry J.P., (in press) Detecting water status in open canopies with thermal ASTER imagery and DART radiative transfer simulation, *Agricultural and Forest Meteorology*, (accepted December 2008).

Serrano, L., & Peñuelas, J. (2005). Assessing forest structure and function from spectral transmittance measurements: A case study in a Mediterranean holm oak forest. *Tree Physiology*, *25*, 67–74.

Sims, D. A., Luo, H., Hastings, S., Oechel, W. C., Rahman, A. F., & Gamon, J. A. (2006). Parallel adjustment in vegetation greenness and ecosystem CO_2 exchange in response to drought in a Southern California chaparral ecosystem. *Remote Sensing of Environment*, *103*, 289–303.

Smith, G. M., & Milton, E. J. (1999). The use of the empirical line method to calibrate remotely sensed data to reflectance.*International Journal of Remote Sensing*, *20*, 2653–2662 (10).

Soudani, K., François, C., le Maire, G., le Dantec, V., & Dufrêne, E. (2006). Comparative analysis of IKONOS, SPOT, and ETM+ data for leaf area index estimation in temperate coniferous and deciduous forest stands. *Remote Sensing of Environment*, *102*(1–2), 161–175.

Strachan, I. B., Pattey, E., & Boisvert, J. B. (2002). Impact of nitrogen and environmental conditions on corn as detected by hyperspectral reflectance. *Remote Sensing of Environment*, *80*, 213–224.

Suárez, L., Zarco-Tejada, P. J., Sepulcre-Cantó, G., Pérez-Priego, O., Miller, J. R., Jiménez-Muñoz, J. C., & Sobrino, J. (2008). Assessing canopy PRI For water stress detection with diurnal airborne imagery. *Remote Sensing of Environment*, *112*, 560–575.

Sun, P., Grignetti, A., Liu, S., Casacchia, R., Salvatori, R., Pietrini, F., Loreto, F., & Centritto, M. (2008). *International Journal of Remote Sensing*, *29*(6), 1725–1743.

Thenot, F., Méthy, M., & Winkel, T. (2002). The Photochemical Reflectance Index (PRI) as a water-stress index. *International Journal of Remote Sensing*, *23*(23), 5135–5139.

Trombetti, G., Riaño, A., Rubio, M. A., Cheng, Y. B., & Ustin, S. L. (2008). Multi-temporal vegetation canopy water content retrieval and interpretation using artificial neural networks for the continental USA. *Remote Sensing of Environment*, *112*(1), 203–215.

Trotter, G. M., Whitehead, D., & Pinkney, E. J. (2002). The Photochemical Reflectance Index as a measure of photosynthetic light use efficiency for plants with varying foliar nitrogen contents. *International Journal of Remote Sensing*, *23*(6), 1207–1212.

Verhoef, W. (1984). Light scattering by leaf layers with application to canopy reflectance modeling: The SAIL model. *Remote Sensing of Environment*, *16*, 125–141.

Verhoef, W., & Bach, H. (2003). Remote sensing data assimilation using coupled radiative transfer models. *Physics and Chemistry of the Earth*, *28*, 3–13.

Verrels, J., Schaepman, M. E., Koetz, B., & Kneubühler, M. (2008). Angular sensitivity analysis of vegetation indices derived from CHRIS/PROBA data. *Remote Sensing of Environment*, *112*(5), 2341–2353.

Wanjura, D. F., Maas, S. C., Winslow, D. R., & Upchurch, D. R. (2004). Scanned and spot measured canopy temperatures of cotton and corn. *Computers and Electronics in Agriculture*, *44*(1), 33–48.

Weiss, M., Baret, F., Garrigues, S., & Lacaze, R. (2007). LAI and fAPAR CYCLOPES global products derived from VEGETATION. Part 2: Validation and comparison with MODIS collection 4 products. *Remote Sensing of Environment*, *110*(3), 317–331.

Weiss, M., Baret, F., Leroy, M., Hautecoeur, O., Bacour, C., Prevot, L., & Bruguier, N. (2002). Validation of neural net techniques to estimate canopy biophysical variables from remote sensing data. *Agronomie*, *22*, 547–553.

Weiss, M., Troufleau, D., Baret, F., Chauki, H., Prévot, L., Olioso, A., Bruguier, N., & Brisson, N. (2001). Coupling canopy functioning and radiative transfer models for remote sensing data assimilation. *Agricultural and Forest Meteorology*, *108*, 113–128.

Winkel, T., Méthy, M., & Thénot, F. (2002). Radiation use efficiency, chlorophyll fluorescence , and reflectance indices associated with ontogenic changes in water-limited *Chenopodium quinoa* leaves. *Photosynthetica*, *40*(2), 227–232.

Wolf P.R. *Elements of photogrammetry* (ed. New York: McGraw-Hill, I.), 1983.

Yang, Y., & Ling, P. P. (2004). Improved model inversion procedure for plant water status assessment under artificial lighting using PROSPECT+SAIL. *Transactions of the ASAE*, *47*, 1833–1840.

Zarco-Tejada, P. J., Miller, J. R., Morales, A., Berjón, A., & Agüera, J. (2004). Hyperspectral indices and model simulation for chlorophyll estimation in open-canopy tree crops. *Remote Sensing of Environment*, *90*(4), 463–476.

Zarco-Tejada, P. J., Miller, J. R., Noland, T. L., Mohammed, G. H., & Sampson, P. H. (2001). Scaling-up and model inversion methods with narrow-band optical indices for chlorophyll content estimation in closed forest canopies with hyperspectral data. *IEEE Transactions on Geoscience and Remote Sensing*, *39*, 1491–1507.

Zarco-Tejada, P. J., Rueda, C. A., & Ustin, S. L. (2003). Water content estimation in vegetation with MODIS reflectance data and model inversion methods. *Remote Sensing of Environment*, *85*, 109–124.

Zhang, Q., Xiao, X., Braswell, B., Linder, E., Baret, F., & Moore, B. (2005). Estimating light absorption by chlorophyll, leaf and canopy in a deciduous broadleaf forest using MODIS data and a radiative transfer model. *Remote Sensing of Environment*, *99*, 357–371.